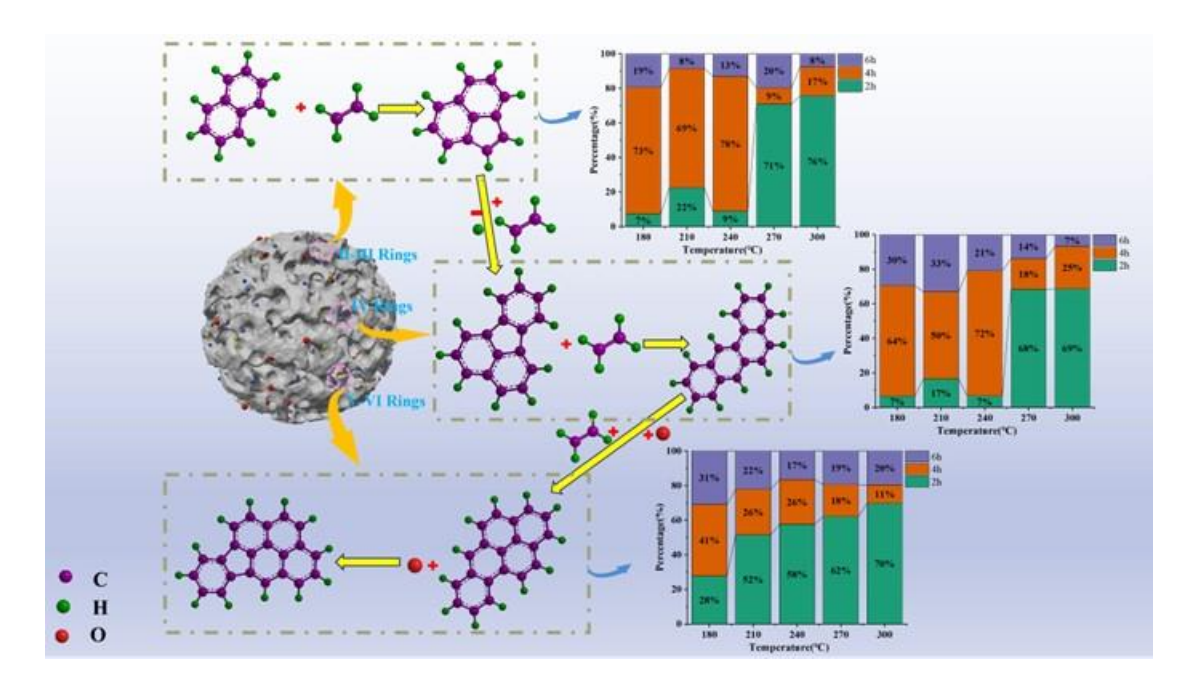
# Distribution Characteristics and Ecotoxicity Assessment of Polycyclic Aromatic Hydrocarbons (PAHs) in Hydrothermal Carbonization Products of Corn Stalks

Hongyu Si,<sup>a</sup> Ming Wang,<sup>a</sup> Chao Xiao,<sup>b</sup> Xiaomei Xie,<sup>c</sup> Junhua Gong,<sup>c</sup> Lijun Yang,<sup>d</sup> Lizeng Peng,<sup>e</sup> Arthur Ernest Dr. Koschany,<sup>a</sup> Xiuxiu Chen,<sup>a,\*</sup> Hewei Yu,<sup>a</sup> Qiang Yao,<sup>e</sup> and Jikai Lu <sup>f,\*</sup>

\* Corresponding authors: Chenxx@sderi.cn (X. Chen), lujikai1996@163.com (K. Lu)

DOI: 10.15376/biores.20.3.5445-5466

#### **GRAPHICAL ABSTRACT**



# Distribution Characteristics and Ecotoxicity Assessment of Polycyclic Aromatic Hydrocarbons (PAHs) in Hydrothermal Carbonization Products of Corn Stalks

Hongyu Si,<sup>a</sup> Ming Wang,<sup>a</sup> Chao Xiao,<sup>b</sup> Xiaomei Xie,<sup>c</sup> Junhua Gong,<sup>c</sup> Lijun Yang,<sup>d</sup> Lizeng Peng,<sup>e</sup> Arthur Ernest Dr. Koschany,<sup>a</sup> Xiuxiu Chen,<sup>a,\*</sup> Hewei Yu,<sup>a</sup> Qiang Yao,<sup>e</sup> and Jikai Lu <sup>f,\*</sup>

Hydrothermal carbonization (HTC) of corn straw causes hydrolysis and pyrolytic reorganization of the carbon skeleton, leading to the formation of polycyclic aromatic hydrocarbons (PAHs). When used as a soil amendment, hydrothermal carbon can lead to soil contamination, increased biotoxicity, and potential harm to ecosystem health. To systematically evaluate PAHs formation mechanisms, single-factor experiments were carried out by treating corn straw under varying temperatures (180 to 300 °C) and durations (2 to 6 h) in a closed batch reactor. PAHs were quantified via gas chromatography-mass spectrometry (GC-MS) with deuterated internal standards. Results revealed that total PAHs concentrations increased by 409%, 66.5%, and 68.3% at 180 °C, 210 °C, and 240 °C (4 h and 2 h), respectively, attributed to intensified dehydration and aromatization reactions under subcritical conditions. Conversely, PAHs levels decreased by 80.4% and 78.1% at 270 °C and 300 °C (4 h and 2 h), likely due to thermal cracking of PAHs macromolecules into low-molecular-weight fragments. Prolonged treatment (6 h and 4 h) reduced PAHs by 62.9 to 70.8% at ≤240 °C, suggesting oxidative degradation pathways dominate over pyrolysis under extended residence time. Mechanistic analysis indicated that optimizing HTC at 270 °C for 4 h achieves a critical balance between carbonization efficiency and PAHs suppression, providing a feasible strategy to mitigate ecotoxicological risks of hydrothermal carbon in soil remediation.

DOI: 10.15376/biores.20.3.5445-5466

Keywords: Hydrothermal carbon; Polycyclic aromatic hydrocarbons; Toxic equivalent; Preparation process

Contact information: a: Shandong Provincial Key Laboratory of Biomass Gasification Technology, Energy Research Institute, Qilu University of Technology (Shandong Academy of Sciences), Jinan, 250014, China; b: Engineering Technology Institute, Jereh Environmental Management Company, Chengdu, 610041, China; c: Shikefeng Chemical Industry Co., Ltd, Linyi, 276000, China; d: Qingdao Guanbaolin activated carbon Co., Ltd, Qingdao, 266300, China; e: Shandong Academy of Agricultural Sciences, Jinan 250100, China; f: College of Engineering, Ocean University of China, Qingdao 266100, China; \*Corresponding authors: Chenxx@sderi.cn (X. Chen), lujikai1996@163.com (K. Lu)

#### INTRODUCTION

Given the advantages of hydrothermal carbon in optimizing soil structure, increasing soil organic matter, and promoting the diversity of soil microbial communities, large-scale soil applications of hydrothermal carbon—either alone or in combination with fertilizers—are inevitable in the future. However, before hydrothermal carbon can be

applied to soils, more in-depth safety assessments and research into safer, more effective processes are necessary. The physicochemical properties of hydrothermal carbon are primarily influenced by reaction conditions, such as temperature and reaction time (He *et al.* 2023). During the hydrothermal process, organic matter undergoes dehydration, decarboxylation, condensation, and cyclization, leading to the formation of polycyclic aromatic hydrocarbons (PAHs). As by-products of hydrothermal carbonization, PAHs have drawn significant attention due to their structural stability and persistence in soil (Hilber *et al.* 2012; Gondek *et al.* 2016).

PAHs are a class of organic compounds composed of two or more fused benzene rings. They are classified into low molecular weight PAHs (2 to 3 rings), medium molecular weight PAHs (4 rings), and high molecular weight PAHs (5 to 6 rings) (Zhang et al. 2021). Biomass undergoes hydrothermal decomposition in an anoxic environment, where the lack of oxygen inhibits complete oxidation reactions, promoting the incomplete breakdown of organic molecules and the formation of PAHs (Nguyen et al. 2019). The small molecular organic compounds generated from the decomposition of biomass components further undergo condensation, cyclization, and restructuring to form PAHs (Hilber et al. 2012). Additionally, the large number of free radicals produced during the hydrothermal process further react, facilitating the formation of PAHs. Due to their carcinogenic, mutagenic, and reproductive toxicity, PAHs pose potential risks to human health and the ecological environment. PAHs are highly persistent in the natural environment, and once they enter it, they are difficult to degrade or remove through natural processes. This persistence allows them to remain in soils, sediments, and water bodies for long periods, and they can spread to wider regions through atmospheric deposition or water circulation (Nikiforova et al. 2019). Studying the formation mechanism, distribution characteristics, and the relationship between PAHs and the physicochemical properties of hydrochar during the hydrothermal carbonization process can further ensure the environmental safety and sustainable use of hydrochar. This research will provide a theoretical basis for optimizing the hydrothermal carbonization process and reducing the generation of harmful by-products, ultimately minimizing the potential negative environmental impact of PAHs (Wang et al. 2018).

The United States Environmental Protection Agency (EPA) has listed 16 PAHs, including naphthalene (NAP) and phenanthrene (PHE), as priority pollutants. These PAHs are present in various hydrocarbons and have become key targets for environmental management due to their persistence and toxicity (Zhao et al. 2020). Several studies have been dedicated to revealing the formation patterns of PAHs under different reaction conditions. Temperature, for instance, influences the PAHs content. In a study on the hydrothermal carbonization of municipal solid waste, Peng et al. (2017) found that increasing the temperature (from 160 to 240 °C) led to higher total PAHs content, but a decrease was observed at 260 °C. Conversely, in a study on the hydrothermal carbonization of pig manure, Lang et al. (2019) found that PAHs content decreased between 180 and 200 °C, but increased again at higher temperatures (220 °C). The temperature also affects the formation of stable carbon during the hydrothermal carbonization process of different feedstocks. Liu et al. (2018) suggested that hydrothermal carbonization enhanced the fuel properties of sludge, but the PAHs content was concentrated in the solid carbon after carbonization. Additionally, temperature influences the abundance of different PAHs. After biomass carbonization, the most abundant PAHs are typically NAP or PHE, and these low molecular weight PAHs account for the majority of the total PAHs content (De la Rosa et al. 2019). Similarly, Jeon et al. (2024) noted that NAP (41.9 to 115.2 μg·kg<sup>-1</sup>) and PHE (55.4 to 144.3 µg·kg<sup>-1</sup>) are the primary contributors to PAHs levels. Biochar from wheat straw and pine needles contain predominantly three-ring and four-ring PAHs (Wang *et al.* 2018). The type and content of these PAHs are not only influenced by temperature but are also closely related to various other conditions during the carbonization process, with reaction time being an important but under-researched variable. Currently, studies on the total PAHs content and specific abundance distribution at different carbonization reaction times are still limited. Especially under high-temperature and long-duration reaction conditions, the formation patterns of PAHs with different molecular weights remain unclear. Further research into the effects of carbonization reaction time on PAHs is essential for providing scientific evidence for evaluating their environmental safety.

Evaluating the PAHs content in hydrothermal carbon derived from corn straw is crucial for mitigating its potential negative impacts when applied to soil. This study investigated the effects of temperature and reaction time on the PAHs content in corn straw hydrothermal carbon through a series of single-factor experiments, with a focus on the total PAHs content and toxicity, as well as the content and toxicity of different PAHs isomers. The aim was to analyze the influence of temperature and time on PAHs formation, explore the generation mechanism and distribution characteristics of PAHs, and identify an optimal combination of reaction temperature and time to reduce PAHs content. By comparing the experimental results with literature values and current standards for PAHs content, this study seeks to provide an effective strategy for reducing toxicity.

#### CHEMISTRY BACKGROUND

Cellulose and hemicellulose, the main components of plant cell walls in lignocellulosic biomass, differ in their structure and function. Cellulose is a linear polysaccharide composed of D-glucose units connected by β-1,4-glycosidic bonds, while hemicellulose is a heterogeneous polysaccharide made up of various monosaccharides (such as xylose, mannose, galactose, arabinose, and glucose) linked by different types of glycosidic bonds. Lignin is a high-molecular compound formed by the random polymerization of three main phenylpropanoid monomers (p-coumaric acid, coniferyl alcohol, and sinapyl alcohol) through phenolic ether bonds and carbon-carbon bonds. In the initial stage (180 to 210 °C), hydrolysis reactions dominate, breaking down cellulose and hemicellulose into soluble sugars and small organic acids, while lignin partially decomposes into monomeric aromatic compounds. In the intermediate stage (210 to 250 °C), the hydrolysis products further decompose, generating more organic acids, aldehydes, and ketones. Lignin continues to break down, producing additional aromatic compounds. This stage is also the primary phase for hydrochar formation, as solid products begin to form. In the high-temperature stage (250 to 300 °C), recombination and condensation reactions occur, leading to the formation of more complex organic compounds, including PAHs. Further degradation products of cellulose, hemicellulose, and lignin undergo polymerization reactions, resulting in solid char. By understanding the chemical reaction mechanisms, the hydrothermal carbonization process can be better controlled to reduce PAHs formation and enhance the environmental friendliness of hydrochar (Fig. 1). The transformation of cellulose and hemicellulose into PAHs under hydrothermal conditions is a critical aspect of this process.

$$(C_6H_{10}O_5)_n \rightarrow n(C_6H_{12}O_6) \rightarrow (C_6H_6O_3) \rightarrow C_5H_4O_2 \rightarrow C_{10}H_8(NAP) \rightarrow C_{14}H_{10}(PHE) \rightarrow C_{28}H_{28} (BaP).$$

The formation process of PAHs from lignin under hydrothermal conditions:

Lignin
$$\rightarrow$$
C<sub>6</sub>H<sub>5</sub>OH + C<sub>6</sub>H<sub>4</sub>(CH<sub>3</sub>)OH $\rightarrow$ C<sub>6</sub>H<sub>5</sub> $\rightarrow$ C<sub>10</sub>H<sub>8</sub>(NAP).

$$C_6H_5OH \rightarrow C_6H_5 \rightarrow C_{10}H_8$$
 (NAP).

$$C_6H_4(CH_3)OH \rightarrow C_{14}H_{12}O \rightarrow C_{14}H_{10}(PHE).$$

At approximately 300 °C, PAHs are generated via a radical mechanism, forming larger aromatic structures. Initially, organic compounds partially decompose into smaller hydrocarbon fragments, such as acetylene, 1,3-butadiene, and H<sub>2</sub>C=CH-CH=CH. These smaller molecules then undergo thermal reactions, where the radicals combine to produce stable, low molecular weight PAHs like naphthalene. As the temperature and residence time increase, these low molecular weight PAHs continue to grow, forming higher molecular weight PAHs through a "zigzag addition process". This process leads to the synthesis of more complex and potentially toxic PAHs, such as BaP and BgP.

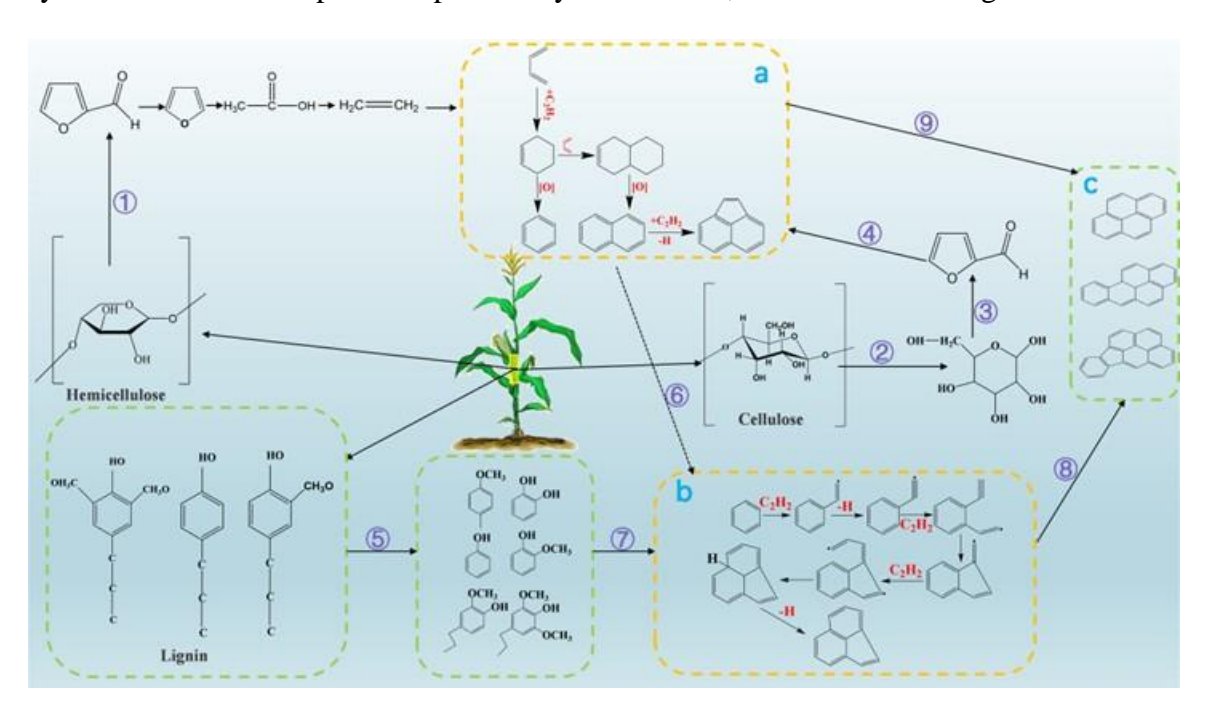


**Fig. 1.** PAHs formation pathways from corn straw hydrothermal treatment. (a) Acenaphthene via Diels-Alder, (b) Acenaphthylene via HACA, (c) BaP and PYR structures. ① Hemicellulose decomposition; ② Cellulose decomposition; ③ Glucose→furfural; ④ Glucose→benzene ring; ⑤ Lignin decomposition; ⑥ Diels-Alder ring→HACA; ⑦ Aromatization; ⑧ ⑨ PAH polymerization.

#### **EXPERIMENTAL**

#### **Chemicals**

The PAHs standard solution (a mixture of 16 PAHs at a concentration of 1  $\mu$ g·L<sup>-1</sup>) and a mixed internal standard solution containing 5 PAHs (including naphthalene-D8, acenaphthene-D10, phenanthrene-D10, chrysene-D12, and perylene-D12, each at a

concentration of 150 mg·L<sup>-1</sup>) were both obtained from Tanmo Quality Inspection Technology Co., Ltd. (Jiangsu, China). Acetone (C<sub>3</sub>H<sub>6</sub>O, purity >99.5%), n-hexane (C<sub>6</sub>H<sub>14</sub>, purity >99%), dichloromethane (CH<sub>2</sub>Cl<sub>2</sub>, purity >99.9%), copper powder (Cu, purity >99.9%), and anhydrous sodium sulfate (Na<sub>2</sub>SO<sub>4</sub>, purity >99%) were purchased from Aladdin Reagent Co., Ltd. (Shanghai, China). All chemicals were of chromatographic grade or higher. Unless otherwise stated, deionized water was used for all aqueous solutions in the experiments.

# **Preparation of Hydrothermal Carbon**

The corn stover utilized in this study was collected from farmland in the suburbs of Jinan City, Shandong Province. The material underwent a preparation process that included washing, air-drying, and pulverization using a high-speed multifunctional grinder (HD2500, LINGSUM, China). The resulting powder was sieved through a 2 mm mesh and stored in sealed bags until use. Hydrothermal carbon was prepared using a 2000 mL electric-heated reaction vessel (GKCF-2L, Gongyi Yingyu High-tech Instrument Factory, Gongyi, China). A 100 g portion of sieved corn stover powder was combined with 500 mL of deionized water, thoroughly mixed, and then transferred into the reaction vessel. The reaction temperatures were set at 180, 210, 240, 270, and 300 °C, with each temperature maintained for 2, 4, or 6 h. After the reaction, the vessel was allowed to cool naturally to room temperature. Solid-liquid separation was conducted using a vacuum filtration system. The resulting hydrothermal carbon solids were dried in an oven until a constant weight was achieved. The hydrothermal carbon samples were labeled as X-Y, where each "X-Y" indicates the reaction temperature and time, respectively.

## **Hydrothermal Carbon Extraction and Chromatographic Conditions**

The extraction and quantification of PAHs in hydrothermal carbon followed the method outlined by Liu et al (2018). A 10 g hydrothermal carbon sample was placed into a 60 mL glass tube, to which 1 g of copper reductant and 40 mL of a mixed solvent (acetone and n-hexane in a 1:1 volume ratio) were added. Subsequently, 1 mL of a PAHs internal standard solution was introduced, containing equivalent ratio concentration naphthalene-D8, acenaphthene-D10, phenanthrene-D10, chrysene-D12, and perylene-D12 at a concentration of 1 µg·L<sup>-1</sup>. The tube was then sealed. The recovery yield for the extraction process was assessed, resulting in an average recovery range of 80.0% to 105.0%. The sample mixture underwent sonication for 30 min, with manual shaking every 5 min to ensure thorough mixing, followed by a 5 min resting period. The supernatant was collected, and the sonication process was repeated four additional times. The combined extracts were concentrated using rotary evaporation to a volume of 60 mL. To eliminate water content, 2 g of anhydrous sodium sulfate was added. The solution was further concentrated to 1 to 2 mL and subjected to purification through neutral alumina and silica columns. Elution was conducted in three stages using 9 mL of a 1:1 mixture of n-hexane and dichloromethane. The resulting eluate was collected, and nitrogen gas was employed to reduce the volume to approximately 1 mL. The purified extract was sealed and reserved for subsequent analysis. Gas chromatography-mass spectrometry (Agilent Technologies 6890N GC, USA) was employed for PAHs analysis under specific conditions: an injection port temperature of 310 °C, an ion source temperature of 230 °C, and a helium gas flow rate of 1 mL/min. Each sample was analyzed three times, see supplementary material Table S1.

### **Polycyclic Aromatic Hydrocarbon Content and Toxicity Evaluation**

The Toxicity Equivalency Quotient (TEQ) of PAHs was determined using the approach outlined by Yin *et al.* (2020). This method utilizes the Toxic Equivalency Factor (TEF) concept to evaluate the total toxicity equivalent relative to benzo(a)pyrene (BaP). The TEF values are assigned to individual PAH based on their relative toxicological potency compared to BaP. By applying these factors, the TEQ of each PAH was calculated, providing an insight into its toxicological significance. The TEQ of PAHs was computed using the following expression,

$$TEQ = \sum (C_i \times TEF_i) \tag{1}$$

where  $C_i$  is the concentration of each PAH, and  $TEF_i$  is the toxicity equivalency factor of each PAH.

# **Analysis of the Physicochemical Properties of Hydrothermal Carbon**

The elemental composition of carbon (C), hydrogen (H), and oxygen (O) in the hydrothermal carbon was determined using an elemental analyzer (Element Analyzer, Elementar-UNICUBE, Germany). The analyzer was operated in CHNS mode for the analysis of carbon, hydrogen, and nitrogen (N) content, and in O mode for oxygen determination.

Fourier-transform infrared (FT-IR) spectroscopy (Thermo Scientific Nicolet is20,USA) was employed to examine the chemical bonds and functional groups present in the hydrothermal carbon molecules. The FT-IR measurements were conducted over a wavelength range of 4000 to 400 cm<sup>-1</sup>.

#### Classification of PAHs

This research focused on identifying the 16 priority PAHs recognized by the U.S. Environmental Protection Agency (EPA), organizing them into three categories based on their molecular weight and the number of aromatic rings. The first category includes PAHs with low molecular weights (II to III rings), such as NAP, acenaphthylene (ACY), acenaphthene (ACE), fluorene (FLU), PHE, and anthracene (ANT).

The second group was made up of medium molecular weight PAHs (IV rings), including fluoranthene (FLT), pyrene (PYR), benzo(a)anthracene (BaA), and chrysene (CHR).

The third group consisted of high molecular weight PAHs (V to VI rings), such as benzo(b)fluoranthene (BbF), benzo(k)fluoranthene (BkF), benzo(a)pyrene (BaP), dibenzo(a,h)anthracene (DhA), indeno(1,2,3-c,d)pyrene (IcP), and benzo(g,h,i)perylene (BgP). Detailed information on the molecular weights, structures, and TEF values for these compounds are provided as supplementary material (Appendix, Table S2).

#### Statistical Analysis

The experimental and measurement data were organized and summarized using Microsoft Excel 2021. Linear regression and chart creation were carried out with Origin 2021. For statistical analysis, one-way analysis of variance (ANOVA) was performed using IBM SPSS 27 software to examine differences both between and within groups, with a significance threshold of 0.05.

#### **RESULTS AND DISCUSSION**

# Effect of Hydrothermal Temperature and Hydrothermal Reaction Time on PAHs Content

The total PAHs content (∑PAHs, consisting of 16 PAHs) ranged from 161 μg⋅kg⁻¹ (270-4) to 2100 μg⋅kg⁻¹ (300-2). According to the U.S. EPA, the maximum allowable PAHs content in biochar for agricultural land use is 6 mg⋅kg⁻¹ (Yang et al. 2021). Although the PAHs content in hydrothermal carbon is below this threshold, it does not imply that the potential long-term environmental impact of biochar can be ignored. At 2 h, ∑PAHs gradually increased with temperature. At 4 h, ∑PAHs first decreased and then increased as temperature rose. After 6 h, ∑PAHs remained largely unaffected by reaction temperature (Table 1). PAHs in hydrothermal carbon exist through two main pathways: On the one hand, PAHs were produced during the hydrothermal reaction due to the solid-phase aromatization process. Although some of these PAHs were volatilized during thermal decomposition, a certain amount remained in the hydrothermal carbon. On the other hand, in the current hydrothermal carbon preparation process, hydrothermal carbon was removed after the reaction system is cooled, which inevitably leads to the PAHs from the reaction system being deposited back onto the hydrothermal carbon during the cooling process.

**Table 1.** PAHs Content of Different Configurations Prepared at 180, 210, 240, 270, and 300 °C for 2, 4, and 6 h

Samples		PAHs (μg·kg <sup>-1</sup> )							
Time (h)	Temperature (°C)	II -Rs	<b>Ⅲ-</b> Rs	IV-Rs	V-Rs	VI-Rs	Total		
	180	11±0.4d	53±1.3d	12±0.2d	96±1.3e	9±0.4d	181±4.0e		
	210	31±1.3c	197±8.2c	22±0.5c	273±6.7c	29±0.4b	553±16.8c		
2	240	9±0.8e	44±1.3d	9±0.4d	327±7.1b	45±2.9a	435±9.5d		
2	270	111±1.4b	377±8.3b	93±1.9b	210±5.6d	27±0.2c	818±18.7b		
	300	600±0.3a	684±5.7a	251±4.7a	531±12.8a	31±0.4b	2097±20.3a		
	180	235±2.5b	413±13.7a	117±6.1a	141±5.6a	16±0.1c	922±43.4a		
	210	321±16.1a	379±18.2b	67±3.0c	128±3.9b	26±0.9a	921±20.5a		
4	240	195±2.2c	275±4.9c	97±2.7b	143±3.8a	23±1.3ab	732±5.1b		
	270	17±1.3e	48±0.9e	24±1.6d	54±1.7c	16±0.2c	160±11.8d		
	300	83±0.1d	201±9.0d	90±0.8b	64±1.3c	21±0.6b	459±9.3c		
	180	115±0.2a	57±0.9d	54±2.1a	106±1.8c	11±0.1b	342±7.1a		
	210	21±0.76c	65±1.7c	44±0.5b	121±2.1b	9±0.3c	260±5.5c		
6	240	17±0.7d	62±1.3c	28±0.4c	90±3.4d	17±0.3a	214±3.3e		
	270	46±3.7b	90±1.8b	19±0.2d	65±2.3e	9±0.5c	230±7.6d		
	300	11±0.3e	119±2.5a	25±1.3c	152±5.1a	6.5±0.1d	314±4.0b		
Time		* * *	* * *	* * *	* * *	* * *	* * *		
Temperature		* * *	* * *	* * *	* * *	* * *	* * *		
Time*		* * *	* * *	* * *	* * *	* * *	* * *		
Temperature									

Values are presented as mean  $\pm$  standard deviation (n=3). Lowercase letters (a to e) indicate statistically significant differences.

<sup>\* \* \*</sup> indicates a correlation < 0.01.

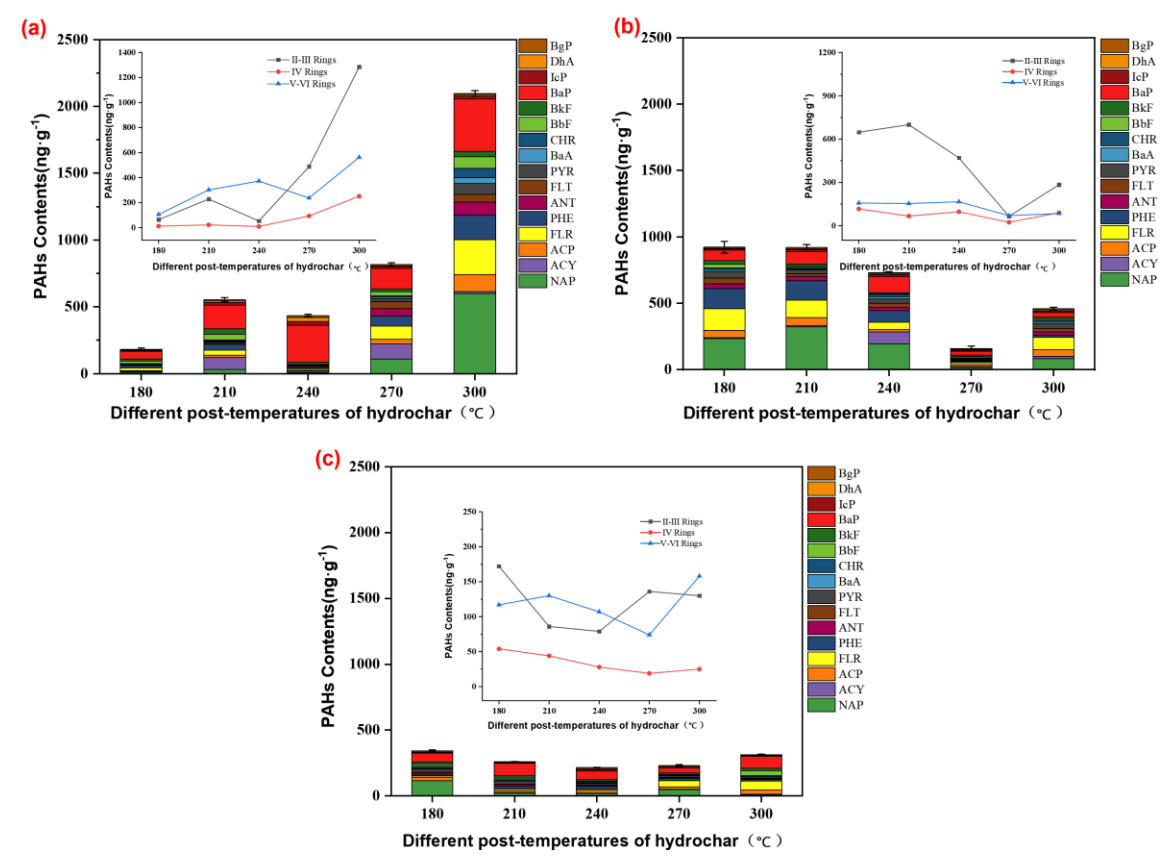
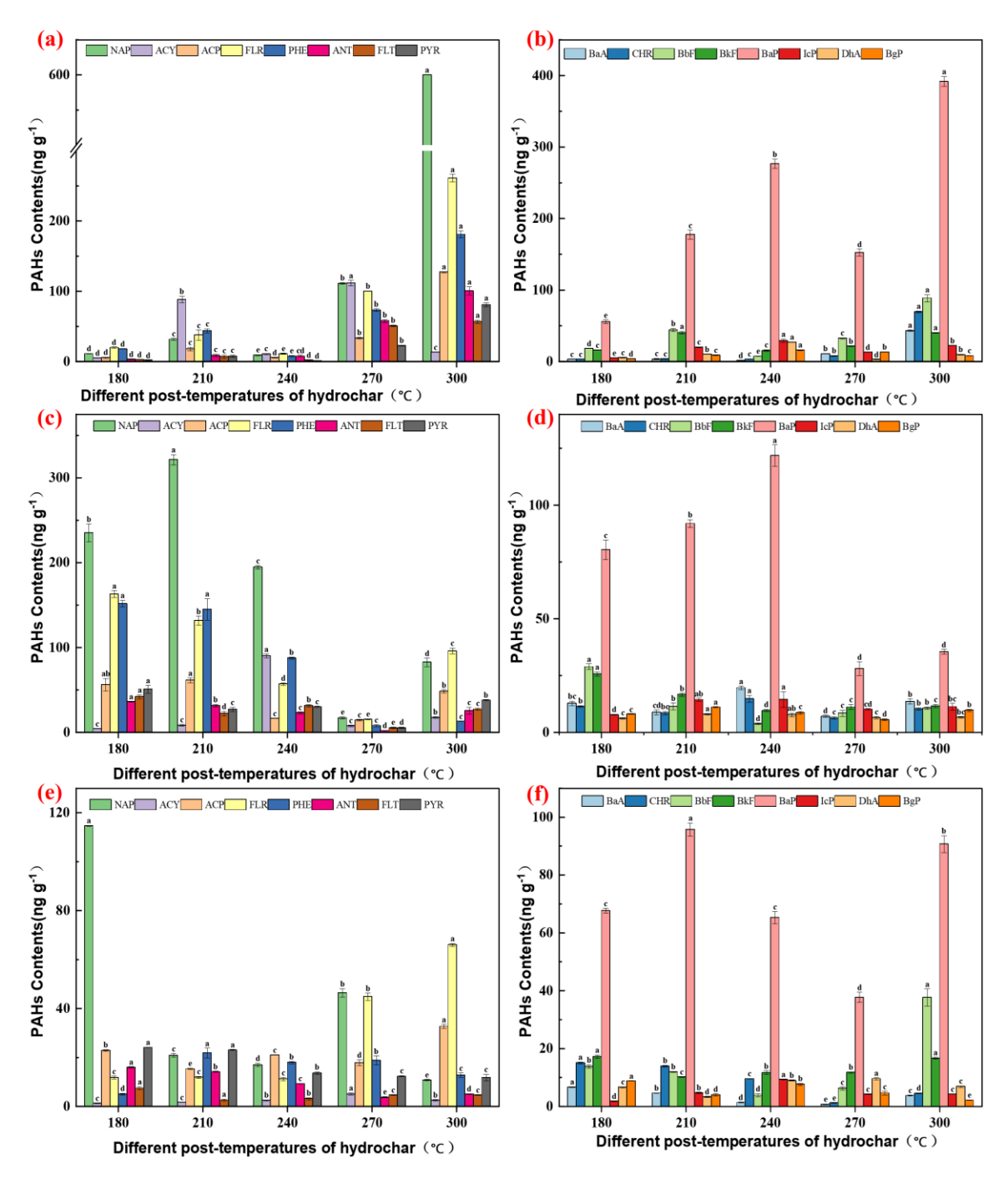


Fig. 2. PAHs content at various reaction times: (a) 2 h reaction time, (b) 4 h, and (c) 6 h

The hydrothermal carbon prepared under a 2 h reaction time is considered to be an initial improvement of soil physical structure, suitable for loose or slightly improved soils (Atallah et al. 2019). At the lowest hydrothermal temperature (180 °C), the total PAHs content in the 180-2 sample was  $181\pm4.0~\mu\mathrm{g}\cdot\mathrm{kg}^{-1}$ , with the highest content of V-Rs PAHs (53.0%). The 180-2 sample was also rich in II-Rs PAHs (only NAP, 6.1%), III-Rs PAHs (29.3%), IV-Rs PAHs (6.6%), and VI-Rs PAHs (5.0%) (Table 1, Fig. 2a). The total PAHs content at this condition was relatively low because the lower temperature prevents complete carbonization, leading to incomplete release of PAHs from the straw (Mohammed et al. 2020). As the temperature was increased to 210 °C, the total PAHs content ( $\Sigma$ PAHs) and the levels of various PAHs types in the 210-2 sample increased. However, the proportions of II-Rs PAHs (5.6%), IV-Rs PAHs (6.0%), and V-Rs PAHs (49.3%) decreased compared to 180-2, while the proportions of III-Rs PAHs (35.6%) and VI-Rs PAHs (5.2%) increased (Table 1). Notably, the ANT content in the III-Rs PAHs increased by 158.8% compared to 180-2, and the reduced release intensity of NAP was attributed to the formation of ANT (Fig. 3a, b). Two possible pathways can explain the formation of NAP. The first is that NAP is released from hydrothermal carbon following the low-temperature formation mechanism of PAHs (Zhu et al. 2017). The second is the conversion of phenol into cyclopentadiene, with cyclopentadiene radicals subsequently forming NAP (Caster et al. 2021). It is noteworthy that in the 240-2 sample, the proportions of V-Rs PAHs (75.2%) and VI-Rs PAHs (10.3%) both increased, with BaP accounting for about 83.0% of the V-Rs PAHs content (Fig. 3a, b). Additionally, the content of ACY in the III-Rs PAHs decreased by 77.6 µg·kg<sup>-1</sup>. Based on previous studies, acetylene appears at temperatures between 200 and 300 °C, suggesting that ACY may originate from the

dehydrogenation-addition of acetylene (HACA) pathway (Reizer *et al.* 2021). The decrease in ACY release indicates that ACY might serve as an intermediate in the formation of other PAHs. In the 270-2 sample, there was an increase in low and medium molecular weight PAHs and a decrease in high molecular weight PAHs. At the highest hydrothermal temperature of 300 °C, ΣPAHs in the 300-2 sample was 2097±20.3 μg·kg<sup>-1</sup>. NAP was the sole representative of II-Rs PAHs, constituting 28.6% of the total PAHs. III-Rs PAHs accounted for 32.6%, with FLU and PHE being the most abundant, comprising 38.2% and 26.5%, respectively, of the III-Rs PAHs. IV-Rs, V-Rs, and VI-Rs PAHs represented 12.0%, 25.3%, and 1.5% of the total PAHs, respectively (Table 1, Fig.3a, b). For V-Rs PAHs, BaP was detected in all samples (180-2, 210-2, 240-2, 270-2, 300-2). BaP is regarded as an indicator of contamination and one of the most carcinogenic PAHs. As the temperature increased, BaP exhibited a sinusoidal fluctuation. Given the presence of BaP in biologically available components, careful attention is required before agricultural use.

The hydrothermal carbon prepared with a 4 h reaction time exhibited ∑PAHs ranging from  $60 \pm 11.80$  to  $922 \pm 43.40 \, \mu g \cdot kg^{-1}$ . Unlike the 2 h reaction, at lower hydrothermal temperatures, the 180-4 sample showed the highest abundance of III-Rs PAHs, accounting for 44.8% (Table 1, Fig. 2b). Due to the dominance of low molecular weight PAHs, which exceeded 70.3%, the proportion of V-Rs PAHs decreased from 53.0% to 15.3%. However, the BaP content increased, and its proportion exceeded 85.2%. As the temperature was increased to 210 °C, the  $\Sigma$ PAHs in the 210-4 sample remained relatively stable (921 ± 20.50 µg·kg<sup>-1</sup>). The content of II-Rs PAHs and VI-Rs PAHs showed an increasing trend, accounting for 34.9% and 2.5%, respectively, while III-Rs, IV-Rs, and V-Rs PAHs showed a decreasing trend, accounting for 41.2%, 7.3%, and 13.9%, respectively (Fig. 3c, d). As the reaction temperature was increased, the PAHs in the hydrothermal carbon underwent splitting and recombination. The extracted PAHs structures displayed a trend of transitioning from low molecular weight PAHs to mediumand high-molecular weight PAHs. II-Rs PAHs could form high molecular weight PAHs through additional "naphthalene-like" reactions (Harrison et al. 2018). In comparison to 210-4, the 240-4 sample showed an overall decrease in low molecular weight PAHs (a reduction of 32.9%) and an increase in medium molecular weight PAHs (an increase of 44.8%), while the content of high molecular weight PAHs remained almost unchanged. Notably, in the 270-4 sample,  $\Sigma$ PAHs dropped to  $160 \pm 11.80 \,\mu \text{g} \cdot \text{kg}^{-1}$ , with V-Rs PAHs, dominated by BaP, accounting for 33.8%. BaP alone made up 62.5% of the V-Rs PAHs (Fig. 3c, d). However, in the 300-4 sample, compared to the 270 °C sample, both the total PAHs content and the content of different PAH types increased. Specifically, II-Rs PAHs accounted for 18.1%, III-Rs PAHs for 43.8%, IV-Rs PAHs for 19.6%, and V-Rs and VI-Rs PAHs accounted for 13.9% and 4.6%, respectively. In comparison to the 300-2 sample,  $\Sigma$ PAHs and the content of different PAH types were reduced in 300-4. With the extension of the reaction time, some PAHs were affected by oxidation, a process that disrupts the original aromatic ring structure, leading to the formation of oxygen-containing compounds or other degradation products, thereby further reducing PAHs content. BaP was detected in all samples (180-4, 210-4, 240-4, 270-4, 300-4). As the temperature increased, BaP showed a cosine-wave fluctuation pattern.



**Fig. 3.** Variation of a content at different temperatures after various reaction times: (a, b) after 2 h, (c, d) after 4 h, (e, f) after 6 h

The trends in PAHs with different configurations in the 210-6 sample, compared to 180-6, and in the 210-2 sample, compared to 180-2, tended to align. Specifically, the content of II-Rs PAHs decreased, while the content of III-Rs PAHs increased. However, the total PAH content ( $\Sigma$ PAHs) in the 180-6 and 210-6 samples decreased overall, with values of  $342 \pm 7.10 \,\mu\text{g}\cdot\text{kg}^{-1}$  and  $260 \pm 5.50 \,\mu\text{g}\cdot\text{kg}^{-1}$ , respectively (Table 1, Fig. 2c). As the temperature increased to 240 °C, low molecular weight and medium molecular weight PAHs in the 240-6 sample showed a decreasing trend, while VI-Rs PAHs significantly increased. During this reaction time, PAH splitting caused high molecular weight PAHs to

decompose and recombine into low or medium molecular weight PAHs. In the 270-6 sample, II-Rs PAHs and III-Rs PAHs increased by 2.71 and 1.45 times, respectively, compared to the 240 °C sample, while IV-Rs, V-Rs, and VI-Rs PAHs decreased by 1.47, 1.38, and 1.89 times, respectively. As the hydrothermal temperature increased, V-Rs PAHs accounted for 48.4%, with BaP having the highest abundance, constituting 59.7% (Fig. 3f). BaP was detected in all samples (180-6, 210-6, 240-6, 270-6, 300-6). Generally, as the temperature increased, BaP showed a sinusoidal fluctuation pattern. According to the Chinese GB18918-2002 standard, the BaP concentration limit for biochar is 3 mg⋅kg<sup>-1</sup> (Harmsen and Rietra 2018). Although the ∑PAHs and BaP levels detected in this study did not exceed the standard, the presence of accumulating PAHs should not be overlooked.

In summary, the changes in PAHs content in hydrothermal carbon can be attributed to two main factors: the decomposition of biomass components and the cleavage and condensation of PAHs. Under shorter hydrothermal reaction times (2 h, 4 h), an increase in temperature tends to elevate the PAHs content in the hydrothermal carbon. However, under longer reaction times (6 h), the total PAHs content is no longer significantly affected by the reaction temperature.

### **Evaluation of PAHs Toxicity**

Due to the persistence of PAHs, their gradual accumulation in the soil poses potential environmental risks. Numerous studies have shown that PAHs not only inhibit normal plant growth but also reduce soil biodiversity (He *et al.* 2023). As PAHs migrate from soil to water bodies and the atmosphere, they may pose adverse effects on human and animal health through skin contact, inhalation, and the food chain. A low concentration does not necessarily imply low toxicity. Whether considering the total  $\Sigma$ PAHs or the individual PAH compounds, it is not possible to accurately determine the degree of PAHs dissolution in materials based solely on their concentrations. In addition to total PAHs content, the toxicity of PAHs is often assessed using the TEQ. The TEF is an effective method for evaluating PAHs toxicity, allowing for a comprehensive assessment of the toxicity of different PAH and providing a comparative value for their overall toxicity (Chen *et al.* 2019).

The results showed that the TEQ value for the 270-4 sample was 39.02 µg·kg<sup>-1</sup>. Although the total PAHs content decreased by approximately 75% when toxicity equivalents were not considered, it is important to note that BaP, which has the highest toxicity equivalent and strong carcinogenic potential, contributed the most to this value (Fig. 4b). BaP is classified as a Group 1 carcinogen by the International Agency for Research on Cancer (IARC). It not only poses a threat to human health but also has the potential to disrupt the ecological balance of other biological communities. The structure of BaP consists of a core five-ring structure (including a central ring) with external benzene rings connected by different chemical bonds. The formation of BaP involves the polymerization of four benzene rings, first forming structures with two benzene rings (such as ANT, PHE, etc.), which then continue to undergo cyclization, hydrogenation, and rearrangement reactions to form the basic structure of BaP (Harrison et al. 2018). Studies have shown that in soils, BaP forms stable complexes with organic matter and minerals, which reduces its bioavailability (Wang et al. 2024). This makes it more difficult for microorganisms or plants to absorb and degrade these pollutants. Research has found that BaP significantly inhibits root growth in plants such as wheat and corn, with root length and weight significantly reduced (Belousov et al. 2021). At high concentrations, BaP can also cause yellowing of plant leaves and decrease chlorophyll content. In polluted soils,

BaP significantly reduces the diversity of bacterial and fungal communities related to soil health. Microbial populations capable of degrading PAHs, such as Pseudomonas and Bacillus, are restricted in growth under high concentrations of BaP (Rabodonirina et al. 2019). Compared to BaP, DhA has a slightly different structure due to the presence of a dihydro group. Although this dihydro group may reduce some of its reactivity, DhA can still be metabolized into substances with strong carcinogenic properties. DhA is a reduction product of BaA and shares a similar structure with BaA, but it contains a hydrogen atom on one of BaA's rings. DhA can be metabolized into carcinogenic metabolites, and as a persistent organic pollutant, it is highly stable in the environment, remaining in soils and water bodies for extended periods. It can enter the human body through the food chain, posing potential health risks. The toxic effects of DhA are weaker than BaP, but it still impacts plant growth, particularly inhibiting root and seedling growth (Ali et al. 2016). Although the formation of PAHs during the hydrothermal process of biomass is unavoidable, future research aimed at reducing the harmful environmental impacts of PAHs should focus on controlling the concentrations of BaP and DhA, with particular attention to BaP levels.

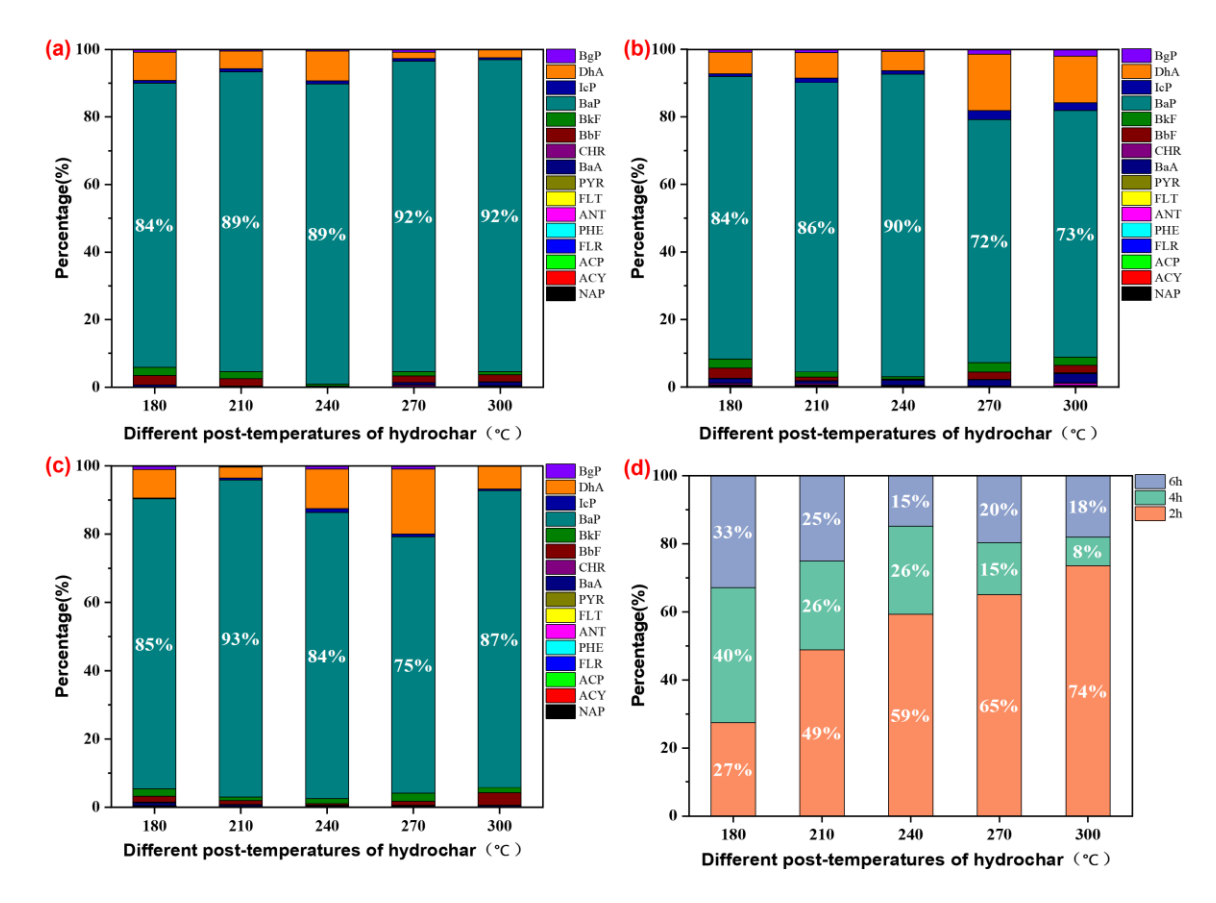


**Fig. 4.** PAHs TEQ after various reaction times: (a) after 2 h, (b) after 4 h, (c) after 6 h, (d) after total 2,4,6 h

The trend in the variation of TEQ values with temperature is primarily due to differences in the content of individual PAH and their corresponding TEF values. For example, compared to the 270-6 sample, the 240-6 sample contained higher levels of V-Rs and VI-Rs PAHs, which have higher TEF values, resulting in a higher TEQ value (Fig. 5c).

After extending the heating time to 6 h at high temperatures, although some aromatic structures remain, many high-toxicity PAHs further decompose or volatilize, leading to a significant decrease in the TEQ value. This is because the degree of aromatization has reached saturation, and the long-term high-temperature treatment results in the recombination or further transformation of aromatic structures, which reduces the overall toxicity. TEQ analysis revealed that the primary factor influencing the toxicity of PAHs in hydrothermal carbon was the presence of high molecular weight PAHs. For example, at a 2 h hydrothermal reaction time, the proportion of V-Rs PAHs in the TEQ at 210 °C and 240 °C was 20.1%, while at 270 °C, VI-Rs PAHs accounted for 23.5% of the TEQ (Fig. 5a). For the 4-h hydrothermal reaction time, at 240 °C, V-Rs PAHs made up 32.2% of the TEO, while at 210 °C, VI-Rs PAHs contributed 25.2% (Fig. 5b). Under the 6 h reaction time at 300 °C, V-Rs PAHs accounted for 25.3% of the TEQ, while at 240 °C, VI-Rs PAHs contributed 32.8% (Fig. 5c). Notably, under the 300-2 hydrothermal conditions, PAHs TEQ accounted for 36.3%, the highest among all the conditions, while under the 270-4 hydrothermal conditions, PAHs TEQ accounted for only 9.0%, making it the least toxic hydrothermal carbon condition in the study (Fig. 5d). Overall, the PAHs toxicity analysis generally follows the same pattern as the PAHs content. Under different conditions, BaP and DhA contributed significantly to the TEQ values of the hydrothermal carbon products, while PAHs with fewer rings, such as NAP, ACY, PHE, and FLT, exhibited lower toxicity.

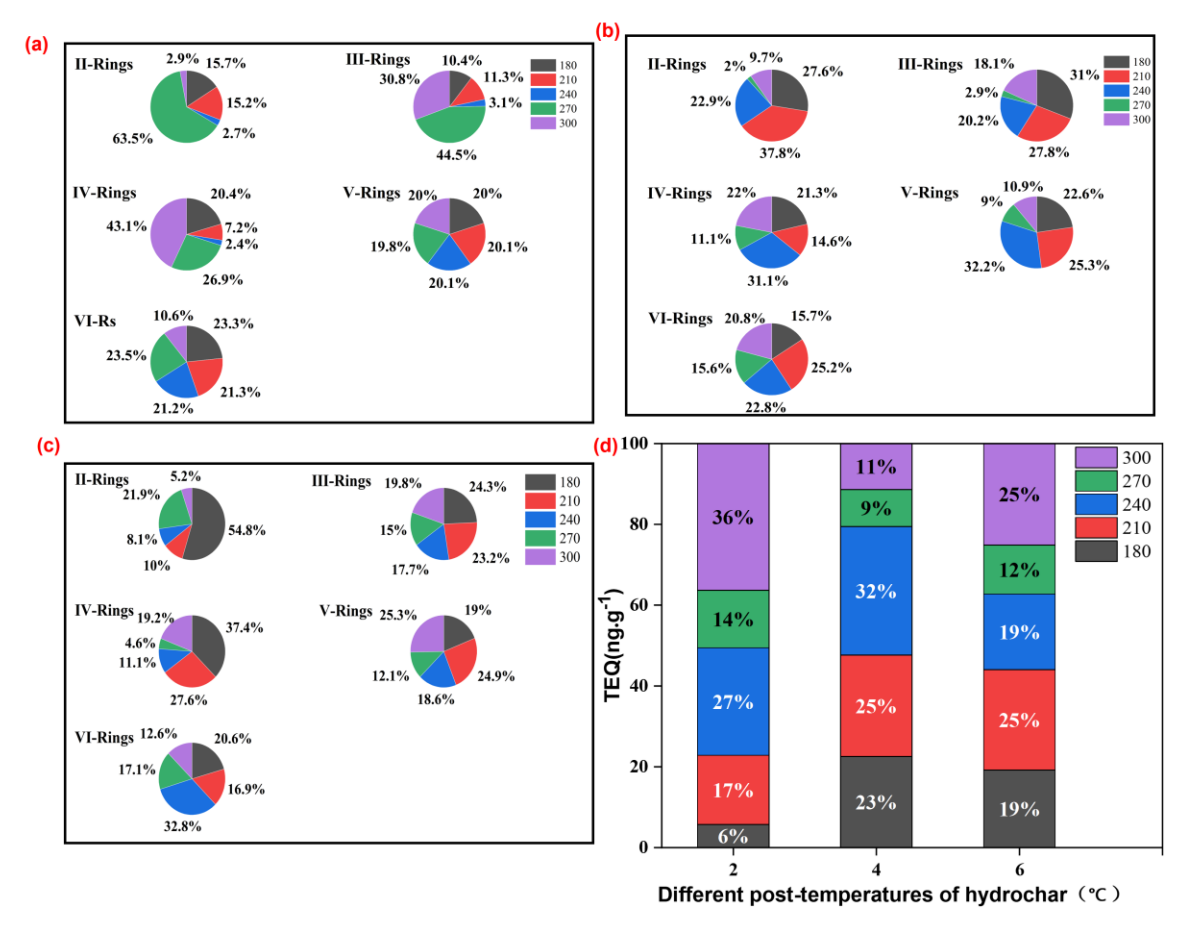


**Fig. 5.** Contribution of different PAH configurations to TEQ. (a) after 2 h, (b) after 4 h, (c) after 6 h, (d) Total TEQ.

# Formation Mechanism of PAHs in Hydrothermal Carbon

To reveal the potential sources and formation mechanisms of PAHs, elemental analysis was conducted, as shown in Table 2. Compared with the raw corn stalk (CS) material, the carbon (C) content in the hydrothermal carbon showed an increasing trend, while the oxygen (O) and hydrogen (H) contents decreased significantly. The ratios of (O+N)/C and O/C also showed a declining trend, which can be attributed to dehydration and decarboxylation reactions. Additionally, the H/C values of CS and 180-2 showed little difference, supporting the analysis in the manuscript that the lower PAHs content in 180-2 was due to incomplete carbonization. Under reaction times of 2 hand 4 h, as the temperature increased, the carbon content rose, while the contents of hydrogen and oxygen decreased. The polarity of surface functional groups (represented by the (O + N)/C ratio) also decreased, and hydrophobicity (represented by the O/C ratio) was reduced. This phenomenon can be attributed to dehydration and decarboxylation reactions (Naderi and Vesali-Naseh 2019). As the reaction time was extended to 6 h, organic molecules in the reaction system continued to undergo dehydration and deoxygenation processes. This resulted in further fixation of carbon in the product, forming a more stable carbon structure (such as aromatization and polymerization), leading to an increase in the carbon content.

Table 2. Elemental Analysis of Hydrothermal Char

Samples					PAHs (ng/g)				
		C (%)	H (%)	O (%)	N (%)	H/C	O/C	(N + O)/C	Yield (%)
CS		49.13	6.16	43.98	0.72	1.49	0.67	0.68	ı
Time (h)	Temperature (°C)								
	180	51.82	5.75	40.29	1.12	1.32	0.58	0.61	62.3
	210	53.25	5.72	39.76	1.18	1.28	0.56	0.54	60.3
2	240	50.96	5.69	42.45	1.56	1.33	0.63	0.34	57.6
	270	54.85	5.62	38.35	1.63	1.22	0.52	0.26	60.3
	300	57.75	5.60	35.05	2.38	1.16	0.46	0.23	50.2
	180	55.75	5.64	37.34	1.26	1.21	0.51	0.52	48.7
	210	55.75	5.74	37.62	0.87	1.23	0.52	0.52	46.6
4	240	55.36	5.79	37.98	0.86	1.25	0.53	0.53	45.0
	270	54.22	5.70	39.29	0.78	1.25	0.55	0.56	43.1
	300	66.11	5.04	26.83	2.01	0.91	0.31	0.33	45.2
6	180	72.98	5.29	19.71	2.01	0.86	0.20	0.23	43.0
	210	70.15	5.20	23.86	0.82	0.88	0.26	0.29	42.4
	240	68.32	5.10	25.46	1.11	0.89	0.28	0.29	42.3
	270	69.89	5.11	23.65	1.35	0.87	0.25	0.27	39.6
	300	69.91	5.04	22.74	2.3	0.86	0.24	0.27	37.2

O/C, (N + O)/C, H/C = Molar ratios

For the aromaticity of hydrothermal carbon, the H/C ratio at two levels is crucial. When the H/C ratio is less than 0.30 or greater than 0.70, the studied material exhibits either a highly condensed or non-condensed structure. All the hydrothermal carbons in this study showed H/C ratios greater than 0.70, confirming that the prepared hydrothermal carbon possessed a high degree of aromatization and carbonization, with no non-condensed structure. PAHs are highly aromatic compounds, and their content typically increases as the H/C ratio decreases. That is, at lower H/C ratios, the molecules in the hydrothermal

carbon are more likely to undergo polymerization reactions to form polycyclic structures. At the same time, the polarity and hydrophobicity of hydrothermal carbon influence the content of PAHs monomers. More polar hydrothermal carbons tend to accumulate lowmolecular-weight PAHs, while more hydrophobic hydrothermal carbons accumulate highmolecular-weight PAHs. For example, in the 180-2 sample, the O/C and (N + O)/C ratios were 0.58 and 0.61, respectively, and the abundance of NAP, FLR, PHE, and BaP was highest under this condition. This is due to the partial decomposition of the biomass components, generating low-molecular-weight PAHs, and on the other hand, to the high polarity of the 180-2 hydrothermal carbon, which leads to a greater accumulation of NAP, FLR, and PHE. Its higher hydrophobicity results in greater accumulation of BaP. A lower O/C ratio indicates fewer oxygen-containing functional groups in the material, making it easier to form condensed aromatic structures, which in turn promotes the formation of PAHs. Over the entire HTC process, as the temperature increases, the carbon structure of the biomass gradually tends toward aromatization, accompanied by the formation of aromatic rings and graphite-like structures (Reza et al. 2015). During this process, any remaining oxygen atoms typically embed into more stable carbon-oxygen structures (such as ether or hemiacetal bonds). Therefore, even as the temperature continues to rise, the oxygen removal efficiency decreases, and the oxygen content stabilizes. In contrast, the removal of hydrogen occurs over a broader temperature range. At higher temperatures, hydrogen is released in the form of gases (such as H<sub>2</sub>) or volatile small molecules (such as CH<sub>4</sub>) (Harmsen and Rietra 2018). This means that although oxygen content stabilizes, the removal of hydrogen may still continue, leading to a further decrease in the H/C ratio. Although oxygen content stabilizes at higher temperatures, the continued removal of hydrogen results in a further decrease in the H/C ratio. The difference in the behavior of hydrogen and oxygen elements explains the observed elemental changes during hydrothermal carbonization. The enhanced aromaticity (decreased H/C ratio) correlates with an increase in PAHs generation, while the stabilization of oxygen content is related to the formation of more stable carbon-oxygen bond structures.

Previous studies have shown that the release of PAHs is related to the aromaticity of hydrothermal carbon. Fourier-transform infrared spectroscopy (FTIR) characterizes the chemical structure of compounds by detecting the characteristic frequencies of molecular vibrations. The trend of PAHs variation can be explained by the following infrared absorbance peaks corresponding to functional groups: C=C stretching vibration (aromatic rings): 1400 to 1600 cm<sup>-1</sup>; C-O and C-O-C stretching vibrations: 1100 to 1300 cm<sup>-1</sup>; -OH stretching vibration: 3300 to 3500 cm<sup>-1</sup>; C-H stretching vibration: 2800 to 3000 cm<sup>-1</sup> (Gao et al. 2013; Zhu et al. 2015). As the temperature was increased from 180 to 300 °C, the intensity of the O-H peak gradually weakened, especially in the 270-2 and 300-2 (Fig. 6a) and 4 h (Fig. 6b) treatments, where the O-H peak nearly disappeared. This indicates that high temperatures intensify dehydration reactions and break down the hydroxyl functional groups in hydrothermal carbon, resulting in a reduction in hydroxyl groups. This trend suggests that prolonged heating at high temperatures destroys the hydrophilicity of hydrothermal carbon, increasing its hydrophobicity, which is conducive to PAHs formation. At 180-2 (Fig. 6a), the C-H peak is quite pronounced, indicating that the hydrothermal carbon still retained a significant amount of aliphatic structures, specifically carbon-hydrogen chains. These aliphatic carbon-hydrogen bonds typically originate from the molecular structures of the original biomass, such as alkyl chains in lignin and cellulose. In this temperature range, due to insufficient thermal energy, the aliphatic structures are not completely degraded, and the C-H bonds do not undergo significant cleavage. Therefore, the resulting polycyclic aromatic hydrocarbons (PAHs) are relatively low in content. As the heating time was extended (Fig. 6b and Fig. 6c), the intensity of the C-H peak further decreased, especially at 270 and 300 °C. This corresponds to the aromaticization trend of PAH formation, as the cleavage of aliphatic C-H bonds leads to the formation of free radicals and smaller carbon-based fragments. These small molecular fragments, driven by thermodynamic forces, undergo polymerization reactions and recombine into stable aromatic structures, generating PAHs. In Fig. 6a, the PAHs content increased significantly with temperature, especially at 300 °C, where the total PAHs content reached 2097 ng·g<sup>-1</sup>. This high content is closely related to the increased intensity of the C=C absorption peak shown in Fig. 6a. The short-term high-temperature treatment promoted the formation of a large number of aromatic structures in the hydrothermal carbon, thereby increasing PAHs generation. In Fig. 6b, the C=C peak remained relatively strong but was somewhat weaker than the 2 h sample. As time progressed, some aromatic structures underwent further rearrangement or decomposition, leading to a decrease in PAHs content. Moreover, PAHs generated at higher temperatures tended to have a higher ring number (such as BaP, BbF), while lower temperatures mainly generated PAHs with fewer rings (such as NAP, ACY, ANT). The enhancement of the aromatic C=C peak is consistent with this, as increased aromaticity at higher temperatures leads to the formation of more high-ring PAHs.

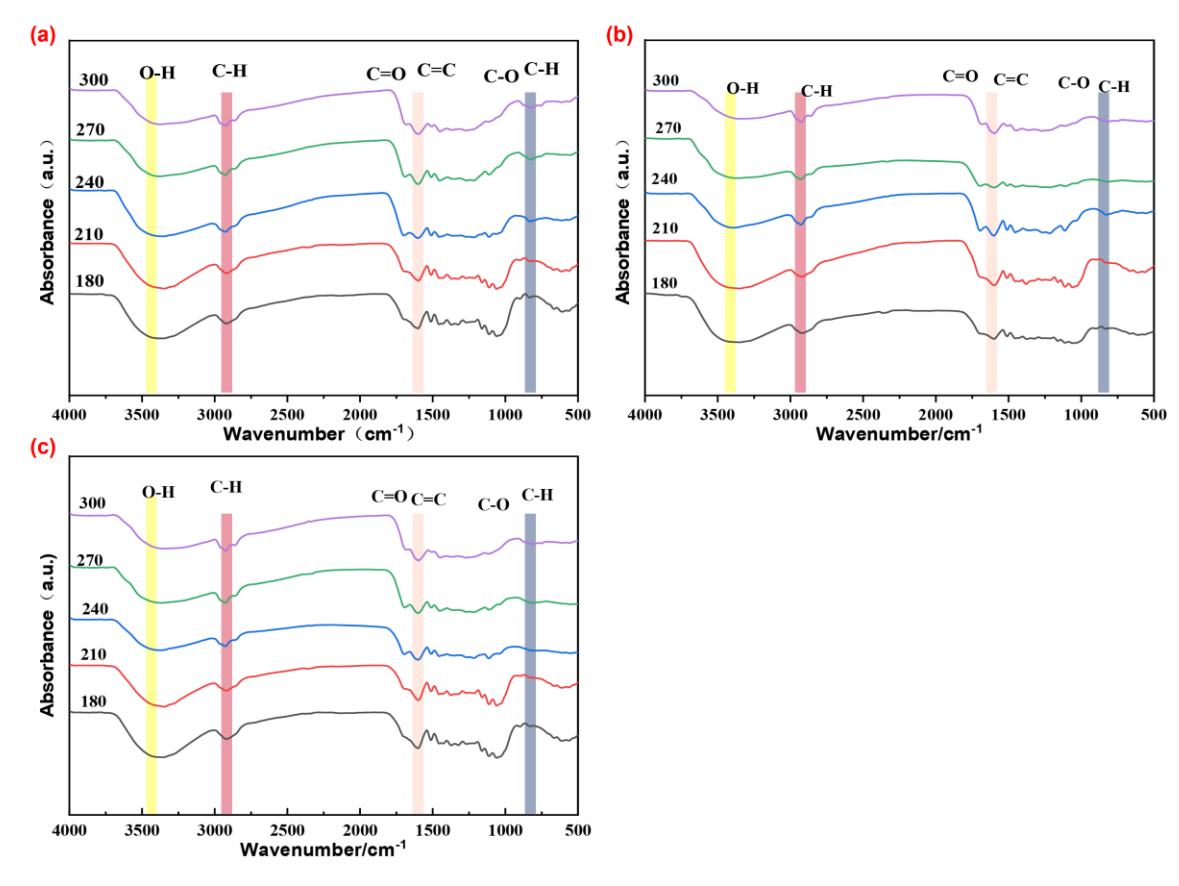


Fig. 6. FT-IR of hydrothermal char at various reaction times: (a) 2 h, (b) 4 h, (c) 6 h

The reduction of C-O and C-O-C functional groups correlated negatively with the increase in PAHs content. As the temperature rose, the cleavage of oxygen-containing functional groups resulted in a gradual loss of hydrophilicity in the hydrothermal carbon, with an increase in aromatic structures, which led to higher PAHs generation. Maintaining a moderate amount of oxygen-containing functional groups can help reduce PAHs formation, thus lowering the environmental risks of hydrothermal carbon. Under the 270-4 hydrothermal conditions, the C=C peak intensity was the lowest, indicating that the hydrothermal carbon under these conditions contained fewer aromatic structures and had not undergone excessive polymerization or aromatization. The lower C-H peak value reflected the organic structure of the hydrothermal carbon, suggesting that this carbon underwent a dehydrogenation reaction during the hydrothermal process, removing some hydrogen and forming a more stable carbon structure. The reduction in C-H bonds usually indicates that the organic matter in the hydrothermal carbon has undergone some oxidation or cleavage processes, reducing the part that is easily degraded by microorganisms while increasing the aggregation of carbon, thereby enhancing the stability of the hydrothermal carbon. A more stable structure can increase the persistence of hydrothermal carbon in soil, reducing the risk of releasing harmful substances. In summary, hydrothermal carbon prepared under conditions of 270 °C for 4 h, with the lowest PAHs content, low C=C and C-H peak values, indicates that this hydrothermal carbon had a relatively simple and stable structure, containing fewer harmful substances. Its good stability and low toxicity make it highly suitable for soil applications, particularly in soil improvement, pollutant adsorption, and promoting soil microbial activity.

#### CONCLUSIONS

- 1. The study examined the content, distribution, and toxicity of 16 priority polycyclic aromatic hydrocarbons (PAHs) in corn straw hydrothermal carbon under different temperature and reaction time conditions. PAHs content ranged from 160.8 to 2097.3 μg·kg<sup>-1</sup>, while TEQ ranged from 78.0 to 849.1 μg·kg<sup>-1</sup>.
- 2. Hydrothermal carbonization produced at 270 °C for 4 h showed significantly lower PAHs levels compared to traditional methods (210 °C for 2 h and 240 °C for 2 h), with reductions of 393.8 and 275.7 μg·kg<sup>-1</sup>, respectively. This suggests that the hydrothermal carbon is more environmentally friendly, reducing health risks and harmful substance accumulation in various applications.
- 3. This study systematically revealed the formation mechanisms and influencing factors of PAHs during the hydrothermal carbonization of biomass, filling a gap in research on the environmental risks of hydrothermal carbonization.
- 4. This study quantified the environmental release potential of PAHs in hydrothermal carbonization products, challenging the conventional perception that "hydrothermal carbon is absolutely environmentally friendly," and emphasizes the necessity of risk assessment before their application to soil or aquatic environments.

#### **ACKNOWLEDGEMENTS**

This study was supported by Shandong key research and development program (2024KJHZ006, 2024TZXD081), The central government guides local Science and Technology Development Fund Projects (YDZX2023007, YDZX2023024), "20 New Items of Universities" funding project of Jinan (202228043, 2021GXRC053), Qilu University of Technology (Shandong Academy of Sciences) Science, Education, Industry Integration and Innovation Pilot Project (2024GH01), and Technology Innovation Guidance Program of Shandong Province (2024LYXZ027).

#### REFERENCES CITED

- Ali, D., Verma, A., Pathak, A. K., Ali, H., and Hans, R. K. (2016). "UVR-induced toxicity of sludge and polycyclic aromatic hydrocarbons on seed germination and seedling growth of *Triticum aestivum* L," *Chemistry and Ecology* 32, 446-459. DOI: 10.1080/02757540.2016.1146711
- Atallah, E., Kwapinski, W., Ahmad, M. N., Leahy, J. J., and Zeaiter, J. (2019). "Effect of water-sludge ratio and reaction time on the hydrothermal carbonization of olive oil mill wastewater treatment: Hydrochar characterization," *Journal of Water Process Engineering* 31, article 100813. DOI: 10.1016/j.jwpe.2019.100813
- Belousov, S., Ovcharenko, A., Kucherenko, S., Gazgireev, K., and Roshchupkin, S. (2021). "Assessment of agricultural ecosystem benzo(a)pyrene pollution on a wheat field model," in: *E3S Web of Conferences* 285. DOI: 10.1051/e3sconf/202128508005
- Caster, K. L., Selby, T. M., Osborn, D. L., Le Picard, S. D., and Goulay, F. (2021). "Product detection of the CH(X(2)Pi) radical reaction with cyclopentadiene: A novel route to benzene," *Journal of Physical Chemistry A* 125, 6927-6939. DOI: 10.1021/acs.jpca.1c03517
- Chen, X., Yang, L., Myneni, S. C. B., and Deng, Y. (2019). "Leaching of polycyclic aromatic hydrocarbons (PAHs) from sewage sludge-derived biochar," *Chemical Engineering Journal* 373, 840-845. DOI: 10.1016/j.cej.2019.05.059
- De la Rosa, J. M., Sánchez-Martín, Á. M., Campos, P., and Miller, A. Z. (2019). "Effect of pyrolysis conditions on the total contents of polycyclic aromatic hydrocarbons in biochars produced from organic residues: Assessment of their hazard potential," *Science of the Total Environment* 667, 578-585. DOI: 10.1016/j.scitotenv.2019.02.421
- Gao, Y., Wang, X., Wang, J., Li, X., Cheng, J., Yang, H, and Chen, H. (2013). "Effect of residence time on chemical and structural properties of hydrochar obtained by hydrothermal carbonization of water hyacinth," *Energy* 58, 376-383. DOI: 10.1016/j.energy.2013.06.023
- Gondek, K., Mierzwa-Hersztek, M., Baran, A., Szostek, M., Pieniążek, R., Pieniążek, M., Stanek-Tarkowska, J. and Noga, T. (2016). "The effect of low-temperature conversion of plant materials on the chemical composition and ecotoxicity of biochars," *Waste and Biomass Valorization* 8, 599-609. DOI: 10.1007/s12649-016-9621-2
- Harmsen, J., and Rietra, R. P. J. J. (2018). "25 years monitoring of PAHs and petroleum hydrocarbons biodegradation in soil," *Chemosphere* 207, 229-238. DOI: 10.1016/j.chemosphere.2018.05.043
- Harrison, R. M., Jang, E., Alam, M. S., and Dang, J. (2018). "Mechanisms of reactivity of

- benzo(a)pyrene and other PAH inferred from field measurements," *Atmospheric Pollution Research* 9, 1214-1220. DOI: 10.1016/j.apr.2018.05.009
- He, M., Dai, P., Lu, J., Kang, Y., Zhang, J., Wu, H., Hu, Z., and Guo, Z.(2023). "Releasing and assessing the toxicity of polycyclic aromatic hydrocarbons from biochar loaded with iron," *ACS Omega* 8, 48104-48112. DOI: 10.1021/acsomega.3c06950
- Hilber, I., Blum, F., Leifeld, J., Schmidt, H.-P., and Bucheli, T. D. (2012). "Quantitative determination of PAHs in biochar: A prerequisite to ensure its quality and safe application," *Journal of Agricultural and Food Chemistry* 60, 3042-3050. DOI: 10.1021/jf205278v
- Jeon, H.-J., Kim, D., Scheufele, F. B., Ro, K. S., Libra, J. A., Marzban, N., Chen, H., Riberio, C., and Jeong, C.(2024). "Occurrence of polycyclic aromatic hydrocarbons (PAHs) in pyrochar and hydrochar during thermal and hydrothermal processes," *Agronomy* 14(9), article 14092040. DOI: 10.3390/agronomy14092040
- Lang, Q., Zhang, B., Li, Y., Liu, Z., and Jiao, W. (2019). "Formation and toxicity of polycyclic aromatic hydrocarbons during CaO assisted hydrothermal carbonization of swine manure," *Waste Management* 100, 84-90. DOI: 10.1016/j.wasman.2019.09.010
- Liu, T., Guo, Y., Peng, N., Lang, Q., Xia, Y., Gai, C., Zheng, Q., and Liu, Z.. (2018). "Identification and quantification of polycyclic aromatic hydrocarbons generated during pyrolysis of sewage sludge: Effect of hydrothermal carbonization pretreatment," *Journal of Analytical and Applied Pyrolysis* 130, 99-105. DOI: 10.1016/j.jaap.2018.01.021
- Mohammed, I. S., Na, R., Kushima, K., and Shimizu, N. (2020). "Investigating the effect of processing parameters on the products of hydrothermal carbonization of corn stover," *Sustainability* 12(12), article 5100. DOI: 10.3390/su12125100
- Naderi, M., and Vesali-Naseh, M. (2019). "Hydrochar-derived fuels from waste walnut shell through hydrothermal carbonization: Characterization and effect of processing parameters," *Biomass Conversion and Biorefinery* 11, 1443-1451. DOI: 10.1007/s13399-019-00513-2
- Nguyen, V. T., Nguyen, T. B., Chen, C. W., Hung, C. M., Vo, T. D., Chang, J. H., *et al*. (2019). "Influence of pyrolysis temperature on polycyclic aromatic hydrocarbons production and tetracycline adsorption behavior of biochar derived from spent coffee ground," *Bioresource Technology* 284, 197-203. DOI: 10.1016/j.biortech.2019.03.096
- Nikiforova, E., Kosheleva, N., and Kasimov, N. (2019). "Accumulation of polycyclic aromatic hydrocarbons in sealed soils and their environmental hazard for Eastern Moscow," *Polycyclic Aromatic Compounds* 41, 1767-1783. DOI: 10.1080/10406638.2019.1696380
- Peng, N., Li, Y., Liu, T., Lang, Q., Gai, C., and Liu, Z. (2017). "Polycyclic aromatic hydrocarbons and toxic heavy metals in municipal solid waste and corresponding hydrochars," *Energy & Fuels* 31, 1665-1671. DOI: 10.1021/acs.energyfuels.6b02964
- Rabodonirina, S., Rasolomampianina, R., Krier, F., Drider, D., Merhaby, D., Net, S., and Ouddane, B. (2019). "Degradation of fluorene and phenanthrene in PAHscontaminated soil using *Pseudomonas* and *Bacillus* strains isolated from oil spill sites," *Journal of Environmental Management* 232, 1-7. DOI: 10.1016/j.jenvman.2018.11.005
- Reizer, E., Csizmadia, I. G., Nehéz, K., Viskolcz, B., and Fiser, B. (2021). "Theoretical investigation of benzo(a)pyrene formation," *Chemical Physics Letters* 772. DOI: 10.1016/j.cplett.2021.138564

- Reza, M. T., Rottler, E., Herklotz, L., and Wirth, B. (2015). "Hydrothermal carbonization (HTC) of wheat straw: Influence of feedwater pH prepared by acetic acid and potassium hydroxide," Bioresource Technology 182, 336-344. DOI: 10.1016/j.biortech.2015.02.024
- Wang, C., Wu, H., Zhao, W., Zhu, B., and Yang, J. (2024). "Effects of polycyclic aromatic hydrocarbons on soil bacterial and fungal communities in soils," Diversity 16. DOI: 10.3390/d16110675
- Wang, J., Xia, K., Waigi, M. G., Gao, Y., Odinga, E. S., Ling, W., and Liu, J. (2018). "Application of biochar to soils may result in plant contamination and human cancer risk due to exposure of polycyclic aromatic hydrocarbons," Environment International 121, 169-177. DOI: 10.1016/j.envint.2018.09.010
- Yang, Y., Wang, J., Wang, Z., Gao, Y., and Pignatello, J. J. (2021). "Abatement of polycyclic aromatic hydrocarbon residues in biochars by thermal oxidation," Environmental Science & Technology Letters 8, 451-456. DOI: 10.1021/acs.estlett.1c00167
- Yin, S., Tan, H., Hui, N., Ma, Y., Tian, L., Sun, N., and Liu, C. (2020). "Polycyclic aromatic hydrocarbons in leaves of Cinnamomum camphora along the urban-rural gradient of a megacity: Distribution varies in concentration and potential toxicity," Science Total Environment 732, article 139328. DOI: 10.1016/j.scitotenv.2020.139328
- Zhang, Z., Ning, S., Li, Q., Sun, M., Lin, J., and Wang, X. (2021). "Levels and risk assessment of polycyclic aromatic hydrocarbons in wood vinegars from pyrolysis of biomass," Chemosphere 278, article 130453. DOI: 10.1016/j.chemosphere.2021.130453
- Zhao, L., Zhao, Y., Nan, H., Yang, F., Qiu, H., Xu, X., et al. (2020). "Suppressed formation of polycyclic aromatic hydrocarbons (PAHs) during pyrolytic production of Fe-enriched composite biochar," Journal of Hazardous Materials 382, article 121033. DOI: 10.1016/j.jhazmat.2019.121033
- Zhu, L., Shi, X., Sun, Y., Zhang, Q., and Wang, W. (2017). "The growth mechanism of polycyclic aromatic hydrocarbons from the reactions of anthracene and phenanthrene with cyclopentadienyl and indenyl," *Chemosphere* 189, 265-276. DOI: 10.1016/j.chemosphere.2017.09.004
- Zhu, X., Liu, Y., Qian, F., Zhang, S., and Chen, J. (2015). "Investigation on the physical and chemical properties of hydrochar and its derived pyrolysis char for their potential application: Influence of hydrothermal carbonization conditions," Energy & Fuels 29, 5222-5230. DOI: 10.1021/acs.energyfuels.5b00512

Article submitted: February 27, 2025; Peer review completed: March 29, 2025; Revised version received and accepted: April 8, 2025; Published: May 15, 2025.

DOI: 10.15376/biores.20.3.5445-5466

#### **APPENDIX**

**Table S1.** Gas Chromatography-Mass Spectrometry Instrument Detection Parameters

Experimental Conditions	Experimental Parameters			
Instrument model	Agilent GC 6890N			
Sample injection method	splitless injection			
Injection volume	1 µL			
Injection port temperature	310 °C			
Type of carrier gas	He			
Carrier gas flow rate	1 mL⋅ min <sup>-1</sup>			
Type of chromatographic column	HP-5 Capillary Column			
Initial column temperature	50 °C			
Column temperature ramp conditions	<ol> <li>Ramp the temperature at 4 °C/min to 220 °C and hold for 5 min.</li> <li>Ramp the temperature at 10 °C/min to 280 °C and hold for 0 min</li> <li>Ramp the temperature at 3 °C/min to 310 °C and hold for 15.5 min</li> </ol>			
Signal acquisition mode	Single Ion Monitoring (SIM)			

**Table S2.** Classification of the 16 priority control PAHs monitored by the U.S. Environmental Protection Agency (EPA)

Rings	Compound	Abbreviation	Molar mass (g/mol)	TEF	Molecular structure
II-Rs	Naphthalene	NAP	128.17	0.001	
	Acenaphthylene	ACY	152.20	0.001	
	Acenaphthene	ACE 152.20		0.001	
<b>Ⅲ-</b> Rs	Fluorene	FLU	166.00	0.001	
	Phenanthrene	PHE	178.23	0.001	
	Anthracene	ANT	178.23	0.01	
IV-Rs	Fluoranthene	FLT	202.25	0.001	
	Pyrene	PYR	202.00	0.001	
	Benz(a) anthracen	ВаА	228.29	0.1	
	Chrysene	CHR	228.29	0.01	

V-Rs	Benzo(b) fluoranthene	BbF	252.31	0.1	
	Benzo(k) fluoranthene	BkF	252.31	0.1	
	Benzo(a) pyrene	ВаР	252.31	1	
	Dibenz( a, h) anthracene	DhA	278.35	1	
VI-Rs	Indeno (1, 2, 3-c, d) pyrene	IcP	276.33	0.1	
	Benzo (g, h, i) perylene	BgP	278.34	0.01	